Temperature variability in a shallow, tidally isolated coral reef lagoon

R. M. McCabe,[1,2] P. Estrade,[1] J. H. Middleton,[1] W. K. Melville,[3] M. Roughan,[4,5] and L. Lenain[3]

Received 30 November 2009; revised 5 August 2010; accepted 31 August 2010; published 4 December 2010.

[1] Temperature data collected in the shallow, tidally isolated reef flat/lagoon of Lady Elliot Island off Queensland, Australia, show marked variability under solar and tidal forcing. Sea level drops below the height of the protective lagoon rim for a few hours during low tide, effectively isolating the remaining water. Because the lagoon is shallow, its temperature change (from diurnal solar forcing and cooling) is amplified. We develop a simple analytical model to predict the time evolution of mean lagoon temperature, beginning with a well-mixed control volume. This approach highlights the asymmetric flood/ebb physics of tidally isolated lagoons. After discussing the response of this model, we compare it with results from two idealized numerical simulations that illustrate differing aspects of lagoon temperature variability under "potential flow" and "prevailing current" situations. The conceptual model captures the essence of lagoon temperature variability and underscores the importance of solar-lunar phasing. However, because of the well-mixed assumption, it cannot reproduce sudden temperature transitions associated with new incoming water masses. Observations show that a slowly progressing thermal wave inundates the lagoon on rising tides. This wave is similar to our "potential flow" simulation in that it is approximately radially symmetric. On the other hand, it appears to advectively replace resident lagoon water, similar to our "prevailing current" simulations. We attempt to account for this behavior with a simple "frontal" modification to our conceptual model. Results show that this frontal model is able to capture the sudden temperature transitions present in the data and offers improved predictive capabilities over the well-mixed model.

Citation: McCabe, R. M., P. Estrade, J. H. Middleton, W. K. Melville, M. Roughan, and L. Lenain (2010), Temperature variability in a shallow, tidally isolated coral reef lagoon, *J. Geophys. Res.*, *115*, C12011, doi:10.1029/2009JC006023.

1. Introduction

[2] Thermal energy balances have been investigated in a range of coastal settings, from continental shelf scales [*Bryden et al.*, 1980; *Lentz*, 1987; *Dever and Lentz*, 1994] to much smaller water masses (e.g., estuaries and bays [*Smith and Kierspe*, 1981; *Uncles and Stephens*, 2001; *Heath*, 1977], mangrove swamps [*Hoguane et al.*, 1999], coral reefs [*Kjerfve*, 1978; *Monismith et al.*, 2006], and recently, tidally influenced rivers [*Monismith et al.*, 2009]). Heat content and temperature variability are of interest for understanding physical processes and because they influence the health of benthic, water column, and other high tropic level (e.g. seabird [*Smithers et al.*, 2003]) communities. Surface ocean temperatures also determine gas solubility coefficients; more CO_2 can dissolve in colder surface ocean waters, thereby impacting seawater chemistry and, in turn, ecosystem health [*Kleypas et al.*, 1999, 2006; *Feely et al.*, 2004].

[3] It is now well known, through a number of studies, that exceeding the thermal stress limits of corals can lead to coral bleaching [*Hoegh-Guldberg*, 1999]. This knowledge, coupled with rising world ocean temperatures, has spurred the development of remote satellite monitoring systems for coral reef health (see, e.g., NOAA's Coral Reef Watch, http://coralreefwatch.noaa.gov). However, ocean temperatures can vary dramatically at individual reefs over small spatial and time scales because of the shallow, sloping [*Monismith et al.*, 2006], and rough bottom topography and variable (tidal, solar, wind) forcing. As one example, *Berkelmans et al.* [2004] were able to predict coral bleaching events best when using maximum temperatures from short (3 day) averaging durations at high spatial (1 km)

[1]Department of Aviation, University of New South Wales, Sydney, New South Wales, Australia.
[2]School of Oceanography, University of Washington, Seattle, Washington, USA.
[3]Scripps Institution of Oceanography, University of California San Diego, La Jolla, California, USA.
[4]School of Mathematics and Statistics, University of New South Wales, Sydney, New South Wales, Australia.
[5]Sydney Institute of Marine Science, Mosman, New South Wales, Australia.

0148-0227/10/2009JC006023

resolution, indicating that brief periods of high temperature can be very stressful to corals. While broad-scale bleaching patterns have been documented [*Berkelmans et al.*, 2004], it is likely that some unexplained reef scale patchiness of bleached corals may be linked to local meteorological and hydrodynamic controls [*Nakamura and van Woesik*, 2001; *West and Salm*, 2003; *Done et al.*, 2003; *Wooldridge and Done*, 2004], although community species type [*Marshall and Baird*, 2000] and specific reef habitats [*Cook et al.*, 1990] can also play significant roles [*Brown et al.*, 2002; *Wooldridge and Done*, 2004; *Baker et al.*, 2008]. Additionally, results from recent coastal metabolic studies suggest that unaccounted for diurnal variability could lead to significant errors in oxygen and carbon system flux and inventory estimates simply because the diurnal variations in shallow systems are so large [*Bates et al.*, 2001; *Yates et al.*, 2007; *Leinweber et al.*, 2009; *Dai et al.*, 2009]. Attempts at addressing spatial scale limitations are underway with recent advances in higher resolution (2–4 km) remote monitoring of the Great Barrier Reef [*Maynard et al.*, 2008; *Weeks et al.*, 2008]. To garner maximum benefit from such systems and to fully comprehend results from biogeochemical experiments, it is clear that further (in situ) understanding of small scale hydrodynamic processes at individual reefs is necessary.

[4] In this manuscript, we present in situ measurements of temperature made over a 13 day period in the shallow lagoon/reef flat of Lady Elliot Island, Great Barrier Reef, Australia. These observations show marked variability over time scales as short as a tidal period. We begin with a brief discussion of the physical features of Lady Elliot Island (section 2) before examining the bulk of our time series data (section 3). Our interest and presentation is focused toward a more general understanding of temperature variability in reef systems. To this point, we offer a simple analytical model (section 4) describing such variability that is based only on generic features of our study site and a well-mixed assumption. We explore the basic theoretical response of this model and then introduce an idealized numerical ocean model to further test the predictive capabilities of the conceptual model (section 5) before attempting to reproduce our lagoon temperature observations. These numerical simulations offer further insight into the processes affecting lagoon temperature evolution. We then compare our prediction with observations and discuss its achievements and shortcomings. The primary features that our well-mixed model consistently misses are sudden temperature transitions associated with flood tide thermal waves. These waves are discussed in more detail in section 6 along with a modified "frontal" version of our conceptual model. Lagoon temperature predictability is improved with this frontal model. A broader discussion of our findings and some limitations appears in section 7 before concluding the paper in section 8.

2. Study Site: Lady Elliot Island

[5] Lady Elliot Island (LEI), a coral cay located off Queensland, Australia, is the southernmost reef of the Great Barrier Reef (GBR) and the site chosen for our study (Figure 1). The island is part of the Capricorn-Bunker group of reefs and is situated on the continental shelf approximately 80 km east of the mainland and only 10 km from the shelf break. Shelf waters in the region are generally well mixed [*Middleton et al.*, 1994]. This part of the Australian coast is topographically complex; just north, the shelf widens dramatically by more than a factor of 2, and to the south, Fraser Island extends almost completely across the shelf. Multiple large-amplitude forcing components exist. Tidal currents are strong (~0.5 m s^{-1}) [see also *Griffin et al.*, 1987], the southeast trade winds consistently blow at around 10 m s^{-1}, the East Australian Current flows just offshore of the shelf break [*Middleton et al.*, 1994; *Kleypas and Burrage*, 1994], and coastal-trapped waves are ubiquitous and are known to scatter in the region [*Griffin and Middleton*, 1986; *Wilkin and Chapman*, 1990; *Merrifield and Middleton*, 1994].

[6] Like other GBR islands, LEI has an intriguing history that includes shipwrecks, introduced goats, and guano mining [*Heatwole*, 1984]. Today, it houses a dive resort with access via a 600 m long airstrip. The island is small, about 1.2 km across from the windward to leeward reef crest/rim (hereafter, rim), making it a tractable site for process-oriented studies. Surrounding average water depth on the shelf is 30–40 m. The windward reef slope (island's east side) is corrugated with grooves that presumably dampen incident wave energy [*Munk and Sargent*, 1948]. Radial channels appear in the coral growth of the 300 m wide windward reef flats. In contrast, the leeward reef flat (island's west side) is only 50 m wide and the slope lacks any groove structure. The two windward reef flats/lagoons (hereafter, lagoons) are separated by an eroding rocky point [*Flood et al.*, 1979; *Chivas et al.*, 1986] that remains dry for much of the tidal cycle implying little exchange occurs between the two bodies. Both lagoons accommodate a variety of coral types and other organisms. The windward reef rim is elevated above the lagoon floors (a sill), offering coral communities protection from the ocean wavefield. This rim is covered by an algal mat. Spring tidal range is approximately 2 m at LEI, and for a portion of low tide, oceanic sea level drops below the reef rim, similar to other GBR islands [e.g., *Ludington*, 1979]. At these times, the remaining lagoon water (nominally 0.5 m deep) is isolated from the ocean, though there is some leakage out through small depressions in the rim.

3. Time Series Observations

[7] A field campaign was initiated at LEI in April 2008 to examine hydrodynamic processes occurring around the island and within the windward lagoons. Here we present only a portion of the data set collected, aimed at providing insight to the lagoon temperature variability and heat budget. The observed spatial structure of lagoon temperature evolution is discussed in section 6.

3.1. Data Sources

[8] Conveniently, LEI houses a land-based meteorological (MET) station that has been operated and maintained by the Australian Bureau of Meteorology (BoM) since 1939. Standard MET variables including wind speed and direction, air temperature, relative humidity, cloud cover, mean sea level pressure, and precipitation are currently recorded every 3 h. Incoming solar radiation, however, is not part of the measurement suite. Instead we present radiation data collected by a Kipp & Zonen CNR1 net radiometer (10% net accuracy) as part of our own MET system. Our MET package also measured three components of wind speed and

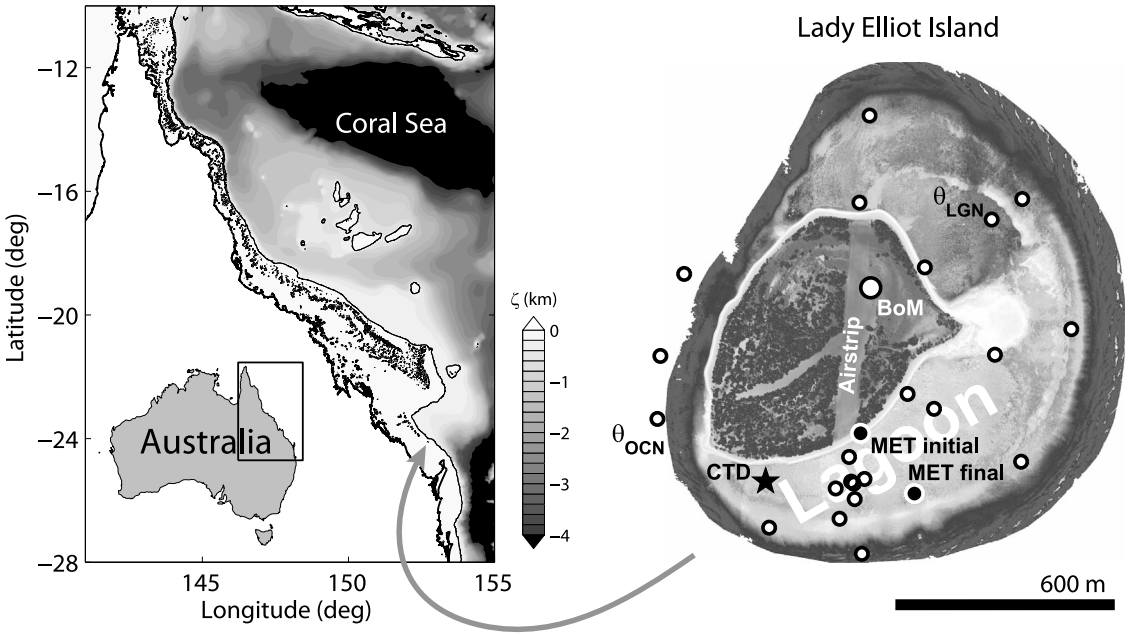

Figure 1. (left) A view of northeast Australia covering the entire Great Barrier Reef, which extends from 10°40′55″S to 24°29′54″S. Axes limits relative to the Australian continent are shown in the lower left inset. The coastline and drying reefs are drawn with a thick black line while the continental shelf break, denoted by the 200 m isobath, is drawn with the thin black line. Drying reef data are ©Commonwealth of Australia, Great Barrier Reef Marine Park Authority (2009). Grayscale bathymetry data come from the GEBCO One Minute Grid (available at http://www.gebco.net). (right) A plan view of Lady Elliot Island (LEI) and key instrument locations including the Bureau of Meteorology weather station (BoM), the two sites for our own meteorological station (MET initial, MET final), and a moored Sea-Bird Electronics Inc. conductivity-temperature-depth recorder (CTD). Small white dots mark locations of individual temperature sensors, including one at ~2 m depth in the "open ocean" θ_{OCN} and another in the north lagoon θ_{LGN} and referred to in section 6. The LEI map was constructed from multiple passes with a portable airborne scanning laser and is described by *Reineman et al.* [2009]. The LEI beach appears as the thin lightly colored strip around the island (intersecting MET initial) and the darkest portions on land are vegetation. For reference, a 600 m scale bar is drawn at the lower right, which is also the length of the LEI airstrip. Grayscale bathymetric shading in the right does not correspond to the color bar in the left. The arrow indicates Lady Elliot Island's location on the Australian shelf in the left.

direction, air temperature, and relative humidity, all at 20 Hz. These data were processed and averaged to 30 min samples. The package was initially positioned on the beach (without radiation measurements) for 10 days at the southern end of LEI (MET initial, Figure 1) facing the predominant southeast trade winds. We then constructed a lagoon-based tower just inside the southern lagoon rim and relocated the MET system (with radiation measurements) there for an additional 10 days (MET final, Figure 1). Thus, incoming and outgoing shortwave and infrared radiation were measured for 10 days over lagoon water.

[9] In addition to the MET system, a Sea-Bird Electronics, Inc. 19*plus* conductivity, temperature, depth (CTD) package, with a Li-Cor photosynthetically active radiation (PAR) unit and a fluorescence and turbidity sensor, was moored in the southern lagoon for 13 days. This system recorded data internally every 5 min. To gain further spatial information on lagoon temperature variability, individual temperature recorders (Onset TidbiT v2; 0.2°C accuracy) were deployed at various locations around the island (Figure 1). Sensors within the LEI lagoon were placed on or near the seabed (~0.5 m depth at low tide and ~2 m depth at high tide), while those outside the lagoon ranged in depth from 2 to 20 m. These sensors also stored data at 5 min intervals.

3.2. Select Observations

[10] Time series (13 days) of various MET data, lagoon sea level, and temperature are shown in Figure 2. This record period captured a marked transformation in atmospheric conditions (Figures 2a–2c) as well as the spring-neap tidal transition (Figure 2d). Although atmospheric temperature changed little (Figure 2a), precipitation (Figure 2a), increased wind speed (Figure 2b), and increased cloud cover (Figure 2c) all occurred during the latter week of observations. Aside from net radiation, all atmospheric data shown were recorded by the LEI BoM station (Figure 1); there was little difference with data recorded by our own MET system. The radiation time series in Figure 2c comes from a combination of net shortwave Q_{sw} and infrared Q_{lw} radiation measured by our radiation sensor (solid black line) along with converted PAR data and an infrared radiation estimate (dashed black line). A linear regression between Q_{sw} values >3 W m^{-2} and concurrent filtered PAR data was used for the shortwave conversion (R^2 = 0.94), whereas a mean value of recorded data

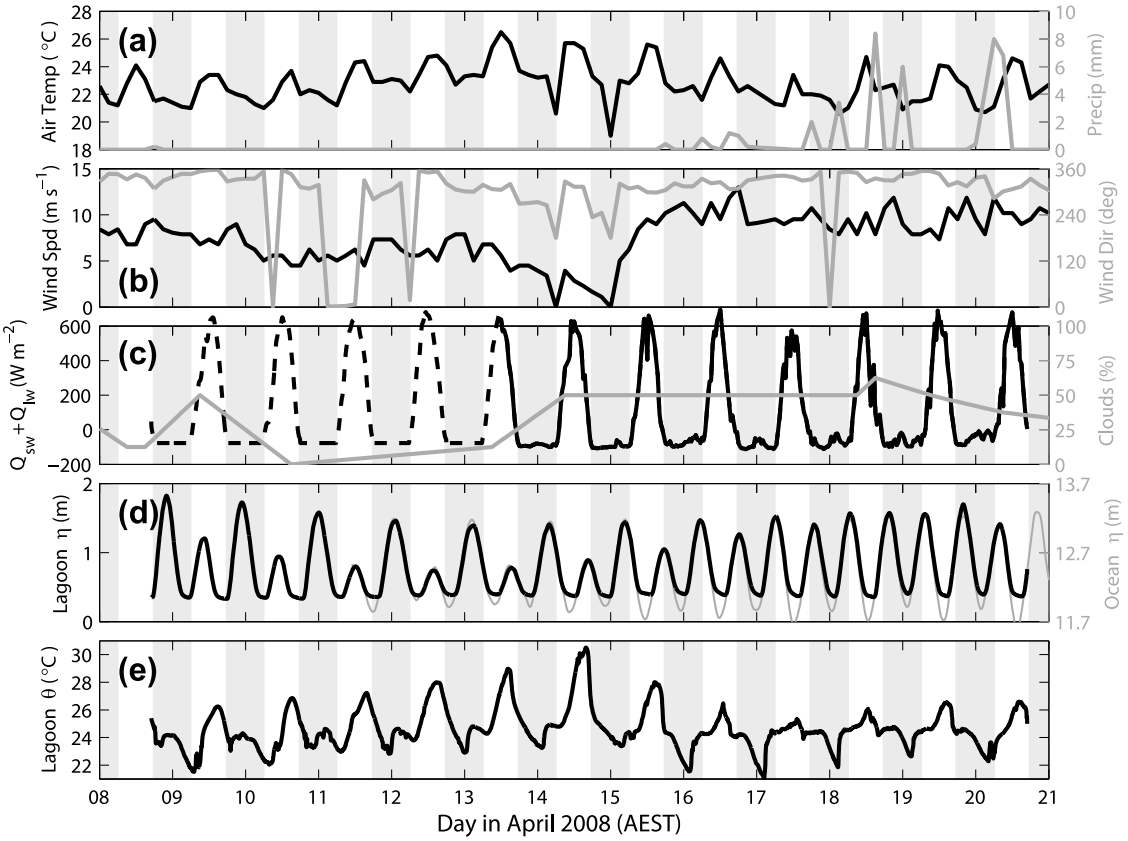

Figure 2. Time series of various data recorded at LEI over 13 days in April 2008. Each panel has alternating vertical white and gray bands that denote day and night, respectively. (a) Air temperature (black) and precipitation (gray), and (b) wind speed (black) and direction (gray), all recorded at 3 h intervals by the Australian Bureau of Meteorology (BoM) weather station on the LEI airstrip. Wind direction in Figure 2b has been rotated to oceanographic convention with 0° pointing north (positive clockwise). (c) Net shortwave Q_{sw} and infrared radiation Q_{lw} (black) and cloud cover (gray). Cloud cover is recorded by the BoM station and is quantified as a percentage of sky coverage; 0% denotes a cloud-free sky. Net radiation comes from a combination of direct measurements (solid black line) and a daytime regression with in situ filtered PAR data and a mean nighttime value (dashed black line). (d) Lagoon water level η (black) and ocean depth (gray) as measured by two different CTD pressure sensors (moored inside and outside the lagoon, respectively), with high-frequency noise filtered out. The ocean depth record begins on 11 April 2008. (e) Observed lagoon water temperature θ measured by the lagoon CTD.

was used for infrared radiation. Daytime average albedo values (not shown) ranged between 11% and 15% (std = 2.7%–8.6%) when our radiometer was over lagoon water (overall daytime mean = 13.5%), although midday values as low as 8% were measured.

[11] The tidally isolated nature of the LEI lagoon is clearly evident in Figure 2d where lagoon sea level changes only slightly for a substantial portion of low tide compared to oceanic sea level. As mentioned earlier, this occurs because ocean sea level drops below the height of the lagoon rim, effectively trapping resident lagoon water. Lagoon temperature data (Figure 2e) show remarkable structure over a variety of time scales. Examination reveals warming during the day (white vertical bands) and cooling at night (gray vertical bands; Figures 2c and 2e) with sharp temperature peaks/valleys associated with day/night low water periods (Figure 2d). Sudden temperature transitions are associated with rising sea level, whereas a smoother decay occurs during ebb tides. In many cases, the temperature extremes are separated by a "shoulder" region where water temperature varies gradually. Daily temperature changes of 4°C–8°C are common in this autumn record. Summertime temperature ranges >12°C have been observed in the LEI lagoon (unpublished data). Solar (Figure 2c) and tidal (Figure 2d) forcing and their relative phasing are primary factors driving the observed lagoon temperature variability. Such features have been documented at other tidally influenced shallow sites (see *Hoguane et al.* [1999] for a similar yet somewhat more complicated example), but to our knowledge have not been fully examined at a shallow coral reef. A warming trend is noticeable over the first half of the lagoon temperature record that is followed by a cooler period (Figure 2e). It is unclear if this lower-frequency change is associated with neap tide (Figure 2d), or the rapid transition in atmospheric conditions halfway through the record. Below we develop a simplified conceptual model to explain lagoon temperature

variability based on the physical features and forcing at the study site. We later evaluate the predictive capabilities of our model.

4. A Well-Mixed Conceptual Approximation

4.1. Control Volume Approach

[12] We approximate the lagoon bounded by an outer reef rim as an idealized control volume V having vertically projected horizontal surface area A_0 (Figure 3). The volume has stationary closed bottom and sidewalls and one open side of area A_{OPEN} at the reef rim, where water may enter or exit the lagoon. The free surface, with irregular area A_{TOP}, is variable. For a reef rim of length y, $A_{\mathrm{OPEN}} = y\,(\eta - \eta_0)$ when the tidally varying lagoon water level η is above the rim ($\eta > \eta_0$). Otherwise, this face is closed and lagoon water is stagnant and isolated from the ocean. As the tide rises, oceanic water eventually flows over the reef rim and into the lagoon, where, for now we assume it is instantly well mixed with resident lagoon water throughout the volume. During ebb, this well-mixed water exits the lagoon over the reef rim. Lagoon water heats and cools because we allow it to absorb solar radiation during the day and radiate energy at night.

[13] Consider the equation governing changes of a tracer θ (temperature in our case) in a Cartesian coordinate system

$$\frac{\mathrm{D}\theta}{\mathrm{D}t} = \frac{\partial\theta}{\partial t} + \mathbf{u}\cdot\nabla\theta = \nabla\cdot(K_\theta\nabla\theta). \tag{1}$$

Here $\mathrm{D}/\mathrm{D}t = \partial/\partial t + \mathbf{u}\cdot\nabla$ is the three-dimensional substantial derivative with $\nabla = (\partial/\partial x, \partial/\partial y, \partial/\partial z)$, the gradient operator, and $\mathbf{u} = (u, v, w)$, a velocity vector with components in the (x, y, z) directions having unit vectors $(\hat{\mathbf{i}}, \hat{\mathbf{j}}, \hat{\mathbf{k}})$, respectively. K_θ is a turbulent diffusivity of θ. Our goal is to apply this equation to the simplified control volume of Figure 3 to better understand processes changing θ in the lagoon. Integrating equation (1) over the lagoon control volume V, making use of incompressibility and the Gauss divergence and Leibnitz theorems [*Kundu and Cohen*, 2008], realizing that the top surface moves at a rate equivalent to the normal flow there and requiring no normal flow through the closed bottom and sidewalls brings us to

$$\frac{\mathrm{d}}{\mathrm{d}t}\int_V \theta\,\mathrm{d}V + \int_{A_{\mathrm{OPEN}}} \theta_{\mathrm{IN/OUT}} u_{\mathrm{IN/OUT}}\,\mathrm{d}A = \frac{1}{\rho_0 c_\mathrm{p}}\int_{A_{\mathrm{TOP}}} Q_{\mathrm{surf}}\,\mathrm{d}A, \tag{2}$$

with $\theta_{\mathrm{IN/OUT}}$ and $u_{\mathrm{IN/OUT}}$ representing sectionally averaged incoming/outgoing water temperature and speed, respectively. On the right-hand side of equation (2), Q_{surf} quantifies time-varying net surface heat flux, ρ_0 is a reference density, and c_p the specific heat of seawater. Equation (2) simply relates the time rate of change of mean lagoon temperature to the flux of heat through the volume's surfaces. Net surface heat flux may be expressed as a sum of many sources and sinks

$$Q_{\mathrm{surf}} = Q_{\mathrm{sw}} + Q_{\mathrm{lw}} + Q_{\mathrm{sen}} + Q_{\mathrm{lat}} + Q_{\mathrm{rain}}. \tag{3}$$

Here Q_{sw} is the net shortwave solar radiation (incident less reflected), and Q_{lw} is the net infrared or "longwave" radiation through the water's surface. Sensible heat flux Q_{sen}, latent heat flux Q_{lat}, and Q_{rain} quantify heat exchange resulting from conduction at the air-sea interface, from evaporation, and the heat gained or lost from precipitation, respectively. Additional heat contributions may arise from exchange with the bottom bathymetry, sediments, and benthic ecosystem Q_{bot} or from advection of differing water masses Q_{adv} (e.g., mean flows) into or out of the volume. The right-hand side of equation (2) results from applying the boundary conditions,

$$K_\theta \left.\frac{\partial\theta}{\partial z}\right|_{z=\eta} = \frac{Q_{\mathrm{surf}}}{\rho_0 c_\mathrm{p}} \tag{4}$$

at the control volume surface $z = \eta$ and

$$K_\theta \left.\frac{\partial\theta}{\partial z}\right|_{z=\zeta} = 0 \tag{5}$$

at the lagoon bottom $z = \zeta$, and assuming $\partial\theta/\partial x = \partial\theta/\partial y = 0$. With equation (5) we have assumed no conduction of heat to the water from the benthos or vice versa ($Q_{\mathrm{bot}} = 0$). Even though we allow ocean water with time-varying temperature $\theta_{\mathrm{IN/OUT}} = \theta_{\mathrm{OCN}}$ to enter the lagoon (and be instantly mixed) we ignore additional heat exchange (e.g., conduction or turbulent transfer) at the lagoon-ocean interface A_{OPEN}. To proceed we need an expression for the sectionally averaged speed of water $u_{\mathrm{IN/OUT}}$ entering or leaving the control volume over the lagoon rim. This is obtained by considering the exchange of mass through our volume's surfaces (negative inward) and is

$$\frac{u_{\mathrm{IN/OUT}}}{A_0/P_0} = -\frac{1}{\eta - \eta_0}\left(\frac{\partial\eta}{\partial t} + E - P\right), \tag{6}$$

with η_0 denoting the height of the lagoon rim, P_0 denoting the lagoon perimeter, and E and P denoting evaporation and precipitation rates, respectively. In reality, we do not expect evaporation or precipitation to significantly alter the amount of water entering or leaving our control volume, but we retain them because they may impact heat storage within the volume. Combining equations (2) and (6) and carrying out the spatial integration gives an equation governing the temporal variability of temperature in the lagoon,

$$\frac{\mathrm{d}}{\mathrm{d}t}(\theta\eta) - \theta_{\mathrm{IN/OUT}}\left(\frac{\partial\eta}{\partial t} + E - P\right) = \frac{Q_{\mathrm{surf}}}{\rho_0 c_\mathrm{p}}. \tag{7}$$

Here $\theta_{\mathrm{IN/OUT}}$ is the temperature of the incoming ocean water θ_{OCN} if lagoon sea level is rising or the outgoing temperature of our well-mixed lagoon water (i.e., θ) if the tide is falling. Because of this asymmetric change in $\theta_{\mathrm{IN/OUT}}$, we end up with two different equations that depend on the lagoon tidal phase:

$$\text{Flood}: \ \theta(t) = \frac{1}{\eta}\int\left(\theta_{\mathrm{OCN}}\frac{\partial\eta}{\partial t} + \theta_{\mathrm{OCN}}(E-P) + \frac{Q_{\mathrm{surf}}}{\rho_0 c_\mathrm{p}}\right)\mathrm{d}t + \frac{\mathrm{const}}{\eta}, \tag{8}$$

$$\text{Ebb and slack}: \frac{\partial\theta}{\partial t} - \frac{(E-P)}{\eta}\theta = \frac{1}{\eta}\frac{Q_{\mathrm{surf}}}{\rho_0 c_\mathrm{p}}. \tag{9}$$

The flood equation results from a straightforward integration of equation (7), while equation (9) may be solved using an integrating factor of $\exp(-(E-P)/\eta)$. Alternatively, if $E - P$ can be safely neglected (as is likely the case), equation (9) may also be directly integrated. The constant of integration

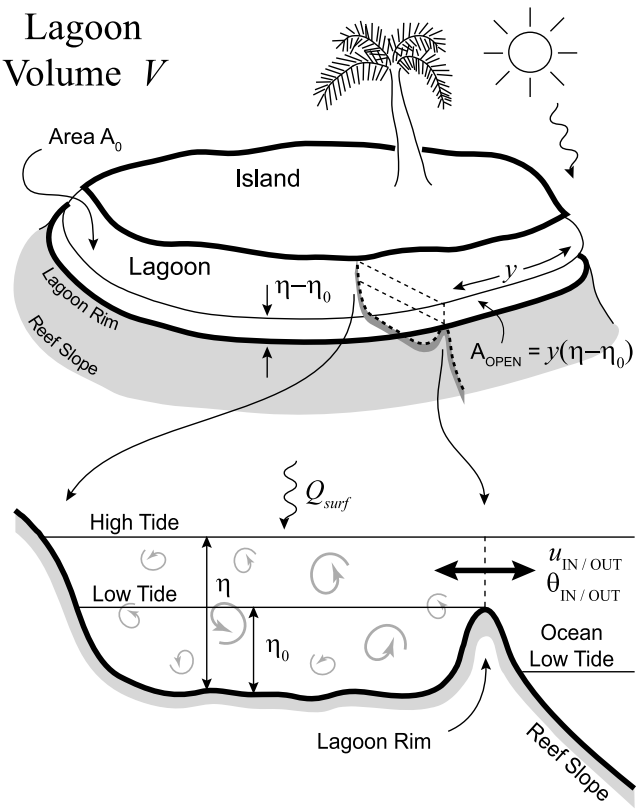

Figure 3. Schematic of the well-mixed control volume approximation for the LEI lagoon. The lagoon has a volume V and vertically projected horizontal surface area A_0. At high tide, the lagoon rim is submerged and the lagoon and ocean are connected. For a portion of low tide ocean sea level drops below the height of the rim effectively isolating the remaining lagoon water. As sea level increases/decreases there is an instantaneous flux of water (at average rate $u_{IN/OUT}$ and with average temperature $\theta_{IN/OUT}$) in/out over the lagoon rim through the face A_{OPEN}. Solar energy heats the water during the day, and radiative cooling occurs at night.

in equation (8) is simply the product of the starting lagoon depth and temperature. Provided we have records of lagoon surface height η, sources/sinks of surface heat flux Q_{surf}, and estimates of (possibly temporally varying) ocean temperature θ_{OCN}, we can use equations (8) and (9) to predict the lagoon temperature over time.

[14] Although our model accounts for changing sea level, we have implicitly limited ourselves to describing relatively shallow lagoons because of our well-mixed assumption [e.g., *Andrews et al.*, 1984]. Similarly, we must focus on relatively small lagoons, where the time of propagation of inflow across the lagoon is short. We evaluate the predictive ability of this simplified model in the sections that follow.

4.2. Basic Behavior of the Well-Mixed Conceptual Model

[15] To test the performance of equations (8) and (9) above, we constructed physically realistic time series of net surface heat flux and tidal height and, for simplicity, chose a constant ambient ocean temperature of $\theta_{OCN} = 24°C$, typical of the southern GBR. In reality, ocean sea surface temperature (SST) will change in time. Our conceptual model can accommodate such changes so long as they are measured. Net surface heat flux was modeled to vary sinusoidally over 12 h of daylight, starting/ending with zero value at sunrise/sunset. A peak value of 400 W m^{-2} (typical for autumn) was prescribed at noon. At night we used a constant negative value such that the net residual heat content of lagoon water would integrate to zero over a full day. We then altered this to incorporate excess heat gain or loss by the water column (as would occur during summer and winter months, respectively). These features are idealized in comparison to our observations (which show a lag/lead of zero net heat flux at sunrise/sunset resulting from reradiation of heat energy by the water), but our current aim is for a general understanding of equations (8) and (9). Tidal height was modeled using amplitudes and phases of the three major constituents (M_2, S_2, and K_1) obtained from a harmonic analysis [*Pawlowicz et al.*, 2002] of 10 min pressure data recorded over 78 days at a site 6 km north of LEI. We modified the values slightly for numerical convenience. This ensured a semirealistic tidal range, spring-neap variability, and diurnal inequality with the highest tides at or near night, as occurs at LEI. Low tides were then clipped and replaced with a constant positive value of 0.45 m to emulate water trapped within the lagoon. Lagoon "leakiness" was not modeled.

[16] Modeled net surface heat flux and tidal height over 21 days are shown in Figure 4 along with predicted lagoon temperature using equations (8) and (9). Three different values of nighttime heat loss appear in Figure 4a: a value representing no net heat gain (neutral state) over a full day (solid black line), half this neutral value (net heat gain, thin gray line), and 1.5× the neutral nighttime value (net heat loss, thick gray line). Corresponding lagoon temperatures appear in Figure 4c and have line styles and colors consistent with the surface heat flux values in Figure 4a. A number of features are evident in Figure 4. Lagoon temperature experiences a spring-neap cycle, with a phase lag, as expected considering the diurnal and semidiurnal forcing frequencies [*Vugts and Zimmerman*, 1975]. It is also apparent that net heat gain/loss results in a warmer/cooler lagoon with the assumed constant temperature ocean acting to dampen lagoon temperature growth. In this case, excess lagoon heat gain gets effectively tempered by the constant temperature ocean water advected and mixed into the lagoon. The largest daily variations occur when there is a net loss of heat from the lagoon (with our chosen input parameters). According to our model, temperature variations of 8°C are possible over only 12 h, even under neutral conditions (Figure 4c, black line). This presents an extreme thermal environment for any benthic lagoon organism. We may expect an even more extreme temperature range during summer conditions.

[17] It is apparent that for a relatively small, tidally isolated lagoon, the main features of temperature variability may be accounted for by our well-mixed, tidal-diurnal model. The model produces the same general temperature structure exhibited by the data (Figure 2) including gradual shoulders between more dramatic day and nighttime peaks and valleys. Even the more erratic features of the prediction share similarities with some of our observations (not shown). The model highlights the asymmetric flood/ebb nature of

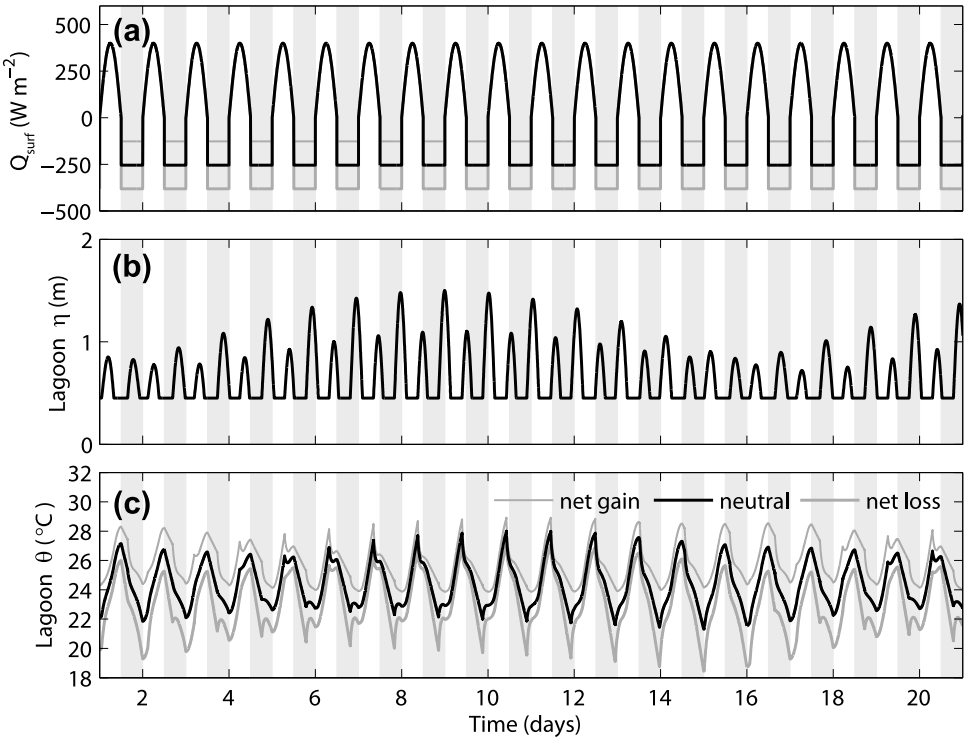

Figure 4. Basic behavior of the control volume temperature response. As in Figure 2, the alternating vertical gray and white bands in each panel denote night and day, respectively. (a) Modeled net surface heat flux Q_{surf} (peak midday value of 400 W m^{-2}) at the lagoon water surface including three nighttime variations: a neutral value (black) such that the residual heat gain integrated over 24 h is zero, 150% of the neutral nighttime value (thick gray) resulting in net heat loss from the water column, and 50% of the neutral nighttime value (thin gray) leading to a net gain of heat by the water column. (b) Modeled lagoon surface elevation η, which incorporates three major tidal constituents (M_2, S_2, and K_1). The low tide water level is clipped at η = 0.45 m to represent isolated lagoon water. (c) Lagoon temperature response resulting from using η in Figure 4b and the three variations of Q_{surf} in Figure 4a in equations (8) and (9) with a constant ambient ocean temperature of θ_{OCN} = 24°C. Line colors and styles in Figure 4c reflect those used in Figure 4a.

shallow tidally isolated lagoons as well as the importance of the solar-tidal phasing. Extreme heating and cooling are likely when low tide occurs near midday and midnight, respectively. Next, we turn to assess how well the model can predict temperature variability in idealized numerical simulations before attempting to reproduce our observed temperature time series.

5. Evaluating the Well-Mixed Conceptual Model

5.1. Reproducing Controlled, Idealized, Numerical Simulations

5.1.1. The Numerical Model, Grid, Bathymetry, and Forcing

[18] We used the Regional Ocean Modeling System (ROMS, Rutgers University version 3.0) for this study [*Shchepetkin and McWilliams*, 2005]. ROMS is a three-dimensional, hydrostatic, finite difference, free surface model that incorporates a "stretched," terrain-following vertical coordinate allowing for higher resolution near the surface and bottom boundaries [*Haidvogel et al.*, 2000]. Horizontal resolution is also adjustable, enabling increased grid density in regions of interest. ROMS solves the primitive equations and has been successful in a number of recent flow topography [*Dong et al.*, 2007; *Estrade and Middleton*, 2010] and heat balance [*Wilkin*, 2006] studies.

[19] Our numerical domain is a stretched Cartesian grid with 140 × 140 grid points in the horizontal and 10 vertical layers. The bathymetry (Figure 5) consists of an idealized circular "atoll" located at the grid center with sidewalls that slope linearly to meet a 15 m deep ocean basin. A shallow lagoon, 0.5 m deep, is carved into the center of the atoll. This lagoon is protected by a rim (or sill) that wets and dries [*Warner et al.*, 2006; J. C. Warner and H. G. Arango, A wetting and drying scheme for ROMS, submitted to *Ocean Modelling*, 2009] with a tidally varying ocean surface height. For our simulations, a critical depth of 0.05 m activates the dry land mask; when the rim water depth is less than this critical value, it dries. All other bathymetric points remain wet and there are four open boundaries. Vertical resolution in the surface water ranges from 0.05 m in the lagoon at low tide to about 1.5 m offshore. Horizontal resolution is 20 m in the lagoon and expands to 570 m offshore. Although this setup omits an island and beach as at LEI, our aim is for the simplest configuration that still retains the essential features of LEI, namely a shallow lagoon separated from the ocean by a wetting-drying reef rim.

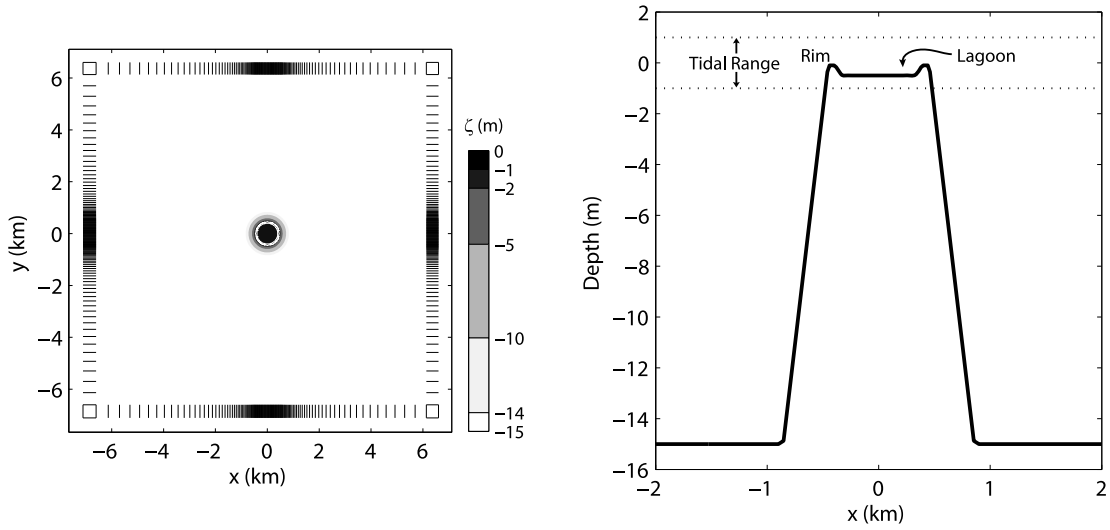

Figure 5. (left) Plan view of the entire model domain and bathymetry ζ, which consists of an isolated, circular "atoll" in the center of a flat-bottom, 15-m deep ocean. Tick marks around the panel edges represent the horizontally stretched grid. White contours show the edges of the atoll rim. Horizontal grid resolution is 20 m in the atoll lagoon and increases to around 570 m offshore. (right) A zoomed, center cross section ($y = 0$) of the idealized atoll bathymetry. The atoll lagoon, rim, and maximum tidal range are all denoted.

[20] We used two different tidal forcing schemes. In the first, termed "potential flow forcing," the sea surface height varies tidally (with a spring-neap cycle specified by the same M_2, S_2, and K_1 constituents as in section 4.2) but remains spatially flat over the entire domain. This has the effect of bringing water in/out radially from all four open boundaries such that the atoll appears as a potential sink/source. This design avoids resident lagoon water from being advected away with a prevailing current. In the second forcing scheme, termed "inertia gravity wave (IGW) forcing," the surface height evolves as a barotropic inertia gravity wave resulting in rotating tidal elliptical currents that can advect lagoon water offshore. Our primary concern is flushing the lagoon. For these simulations, we again used the same three tidal constituents as in section 4.2 and assumed northward propagation for all of them. This results in a tidal ellipse with a large ratio of major-to-minor axes. Further details of the IGW forcing may be found in the work of *Estrade and Middleton* [2010]. In both forcing cases open boundary conditions for the free surface and depth-averaged momentum are given by the *Chapman* [1985] and *Flather* [1976] formulations. Three-dimensional fields of velocity and tracers are treated with a radiation boundary condition [*Marchesiello et al.*, 2001]. Highly viscous and dissipative sponge layers six-grid points wide are also used along all open boundaries. Net surface heat flux is applied equally over the entire model domain and is idealized in the same manner as described in section 4.2 (Figure 4a), with 12 h of daylight, a peak value of 400 W m^{-2} prescribed at noon, and zero net heat gain or loss over a 24 h period. We used a shallow water drag coefficient of 2.5×10^{-3}, a large vertical viscosity and diffusivity of 1×10^{-3} m^2 s^{-1}, and horizontal viscosity and diffusivities of 1 and 2 m^2 s^{-1}, respectively. There is no surface wind stress or initial stratification and the model is spun up from rest over 1 day.

5.1.2. Numerical Results

[21] A much simpler numerical domain can be used to investigate heat balances in an idealized basin. However, our present atoll configuration allows us to illustrate some complications that may arise in natural settings. Consider first the potential flow case (Figure 6), where water is effectively trapped in the lagoon, albeit with some radial exchange. Diurnal heating and cooling of lagoon water is clearly evident, but additional small-scale spatial temperature gradients appear near the lagoon rim over its sloping bathymetry. The best examples are during low tide when the lagoon is isolated from the ocean (Figures 6c, 6d, 6h, 6i, and 6j). Excessive heating/cooling, by as much as 2°C, occurs in the shallowest water near the rim (both inside and outside) during day/night. Apparently small depth changes can lead to dramatic SST variability in shallow settings; recall that our model lagoon is only 0.5 m deep at low tide. Such localized zones of heated or cooled water will impact lagoon-wide temperature structure and can lead to small-scale thermal flows [*Monismith et al.*, 2006]. *Hoguane et al.* [1999] had to incorporate a small heating/cooling "box" in their theoretical model of a mangrove swamp to account for similar SST variability just outside their sill. For a small isolated island with a steep slope, the outer rim heating/cooling should be less significant since open ocean currents can advect nearshore water away. However, thermal flows could occur within the isolated lagoon as suggested by Figure 6. Turning to the time series of lagoon temperature in Figure 6n, we see that our theoretical prediction (red line) agrees extremely well with the numerically simulated lagoon temperature (thick black line), capturing all the essential features of the temperature signal. In this case, ROMS lagoon temperature was extracted from a station located one-third of the way into the lagoon (gray dot, Figure 6d) where advection of ambient ocean water over the

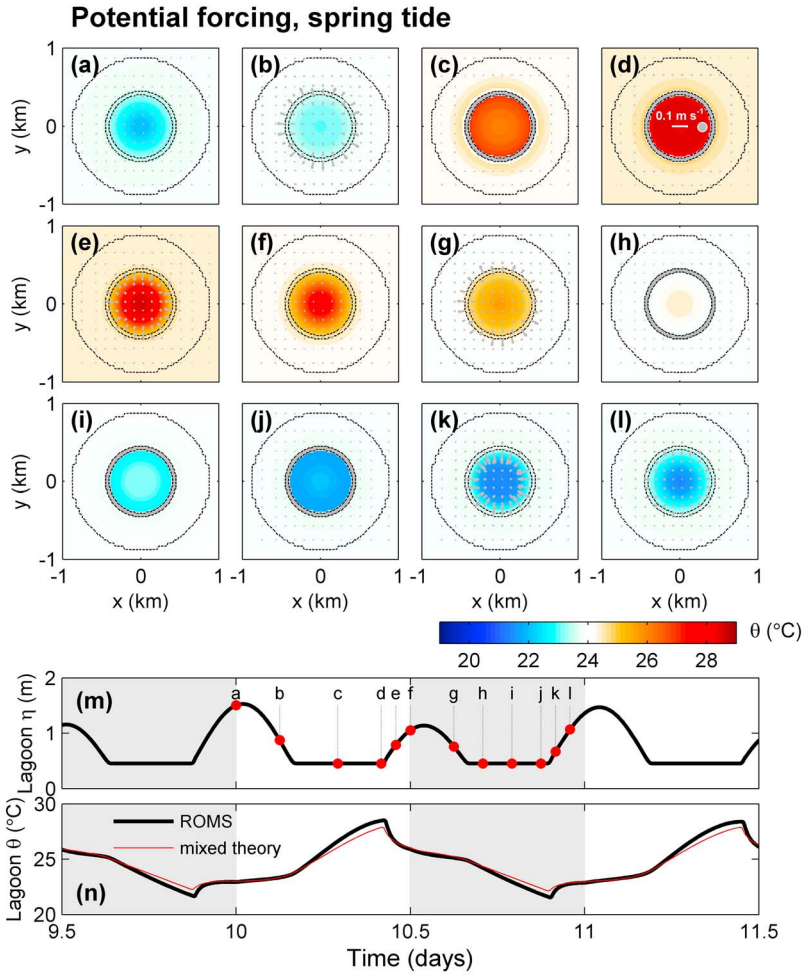

Figure 6. (a–l) Select ROMS plan view SST and surface velocity maps for the potential flow forcing at spring tide. The lagoon rim is denoted by the two innermost concentric black circles and the seaward extent of the atoll slope is drawn as the outermost black circle. The lagoon rim appears gray when dry. For clarity, velocity vectors (gray arrows) are drawn only at every sixth grid point but are omitted when <0.001 m s^{-1}. A white scale vector at the center of Figure 6d represents 0.1 m s^{-1}. (m) Timing of each SST/velocity map relative to the lagoon depth. (n) Short time series of ROMS model (thick black line) and well-mixed conceptual model (thin red line) lagoon temperature. The ROMS temperature time series comes from a station approximately one-third of the way into the lagoon, indicated with the gray dot in Figure 6d. The well-mixed model temperature time series was calculated using Q_{surf} and η from Figures 4a and 4b and θ_{OCN} from offshore of the numerical atoll in equations (8) and (9). Alternating gray/white vertical shading in Figures 6m and 6n represent night/day, respectively.

rim can modify the lagoon thermal structure. We chose this location because it became evident that water near the center of the lagoon experienced little or no influence from the outer ocean despite large tracer diffusivity (and hence a lagoon-wide average temperature was deemed a misleading comparison). This is because radial currents get progressively weaker as one approaches the lagoon center. Slight differences do exist between the conceptual and numerical models and result from the numerical lagoon not satisfying the stringent, well-mixed assumption described in section 4.

[22] Numerical results from the IGW forcing case are illustrated in Figure 7 with the same SST snapshot times as shown in Figure 6. Here prevailing ocean currents (gray arrows) advect lagoon water offshore away from the lagoon (Figures 7e, 7f, 7k, and 7l), reminiscent of the wind-forced case described by *Ludington* [1979]. This has a profound impact on lagoon temperature variability as illustrated in both the snapshots (Figures 7a–7l) and the temperature time series (Figure 7n). Comparisons with Figure 6 show that lagoon temperature extrema in the IGW case are larger in magnitude and the flood tide temperature transitions following those extremes are more severe than in the potential flow scenario. The IGW run exhibits larger temperature extremes because relatively constant temperature ocean water replaces resident heated/cooled lagoon water. Thus, new heating/cooling phases start from the less extreme ambient ocean temperature instead of from anomalously cooled/heated water, as in the potential flow case. This allows

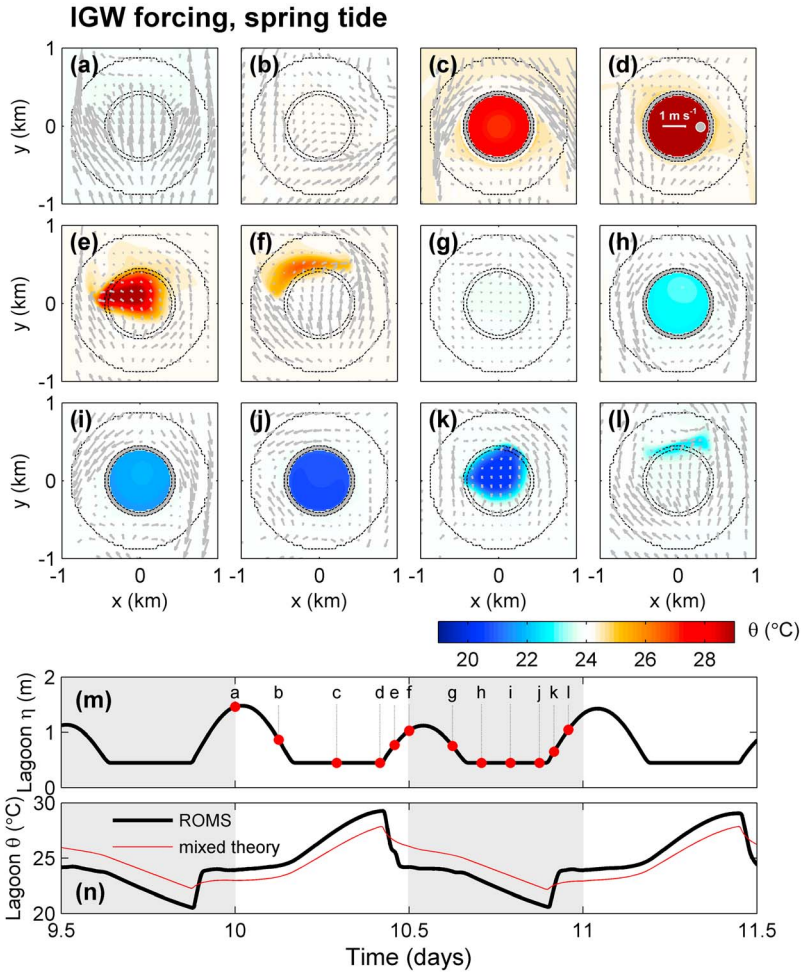

Figure 7. The same as Figure 6 except for the inertia gravity wave forcing. In this case the white scale arrow in Figure 7d represents 1 m s^{-1}. For clarity, gray velocity vectors are drawn only at every sixth grid point but are omitted when <0.01 m s^{-1}.

for excessive heating/cooling during the day/night following the change in water mass. Sharper temperature transitions in the IGW case clearly result from advection in of the ambient ocean water mass (Figure 7). As a result, our prediction (Figure 7n) still captures the general temperature trend, but it has only mediocre performance when prevailing ocean currents replace lagoon water instead of mixing with it locally.

[23] These two numerical experiments illustrate important features relevant for natural systems. First, small depth changes can result in significant horizontal temperature differences in shallow systems, with the potential for thermal flows in isolated settings. Additionally, in situations where lagoon water is "advectively replaced" we may expect enhanced diurnal temperature variability with higher maximum and lower minimum temperatures than if lagoon water were mixed with incoming ocean water. We next turn to our LEI temperature observations with the above insights in mind.

5.2. Reproducing Lagoon Temperature Observations

[24] To compare predictions of lagoon temperature with our data, we must first construct time series of net surface heat flux Q_{surf}, ambient ocean temperature θ_{OCN}, and evaporation E and precipitation P rates. Precipitation was recorded at the BoM MET station (Figure 2a), and we use a time series of temperature recorded from 2 m depth at the southwest side of the island for θ_{OCN} (location in Figure 1). We can relate the evaporation rate E to Q_{lat} as $E = Q_{lat}/(\rho_0 L_E)$, with $L_E \sim 2.5 \times 10^6$ J kg^{-1} as the latent heat of vaporization [e.g., *Stewart*, 2008], and can, in turn, calculate both Q_{lat} and Q_{sen} from eddy-covariance of high-resolution atmospheric and surface ocean data. Alternatively, Q_{lat}, Q_{sen}, and Q_{rain} may be estimated with bulk formulations [e.g., *Fairall et al.*, 1996; *Pawlowicz et al.*, 2001], which we use here. Heat exchange with the bottom Q_{bot} has largely been ignored in most energy budget studies, and even when it has been measured, Q_{bot} typically contributes little to the heat content of the overlying water column (a mudflat example is given by *Heath* [1977]). Bottom heat fluxes are, however, likely important for the benthic ecosystem [*Fabricius*, 2006; *Jimenez et al.*, 2008]. With equation (5), we ignored Q_{bot} in our heat budget. Similarly, we discard any additional advective contributions Q_{adv} beyond what is captured by the second term in equation (7). Individual surface heat flux components are shown in Figure 8. The atmospheric transition on 15 April 2008, characterized by increased wind speed (Figure 2b), is also clearly evident in

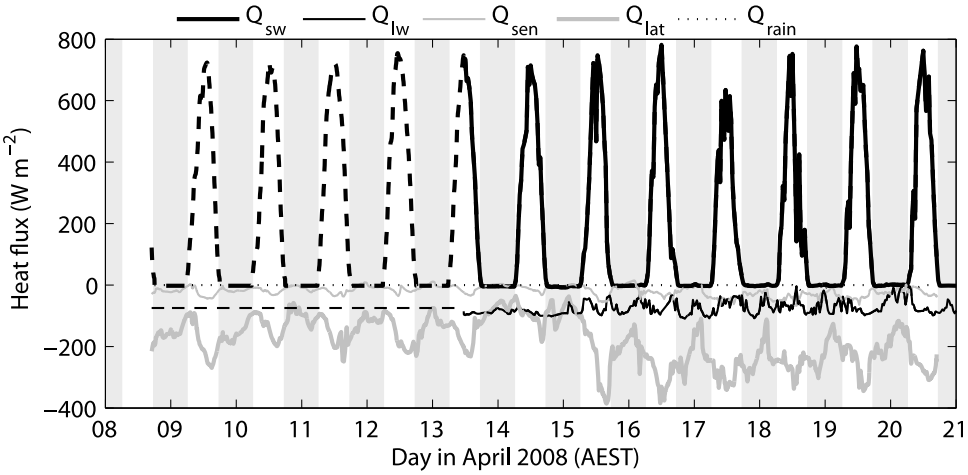

Figure 8. Surface heat flux components over the measurement period including net shortwave radiation Q_{sw}, net infrared radiation Q_{lw}, sensible heat flux Q_{sen}, latent heat flux Q_{lat}, and the heat flux associated with rainfall Q_{rain}. Dashed portions of Q_{sw} and Q_{lw} represent approximations; for Q_{sw} a regression with PAR data was used ($R^2 = 0.94$), whereas the dashed portion of Q_{lw} is simply the mean of its recorded value over the latter part of the experiment. Alternating white/gray vertical bands indicate day/night.

the latent heat flux record (thick gray line, Figure 8). Strong winds are very effective at extracting heat from the shallow lagoon through evaporation. In fact, evaporation represents the largest sink of lagoon thermal energy. Even though all other heat loss mechanisms show little change throughout the experiment (e.g., compare Q_{lw} from 13 to 14 April with that after the 15 April transition), there is on average, an additional 100 W m^{-2} of heat energy lost through evaporation during the latter half of the record when compared to the initial half. For reference, the autumn seasonal mean evaporative flux for this region is 180 W m^{-2} [*Weller et al.*, 2008], not too different from the 150 W m^{-2} mean value observed before the 13 April wind relaxation. Diurnal variations in Q_{lat} also appear more pronounced during the latter portion of the experiment.

[25] Time series of net surface heat flux, lagoon depth, and various measures of temperature are shown in Figure 9. The mean net surface heat flux over the record period is −87 W m^{-2}; approximately −36 W m^{-2} before the 15 April transition and −148 W m^{-2} after (Figure 9a). It is not surprising that the additional −100 W m^{-2} evaporative flux is reflected in the latter half of the net surface heat flux time series. A ~2°C cooling of the lagoon water column (mean over all lagoon temperature sensors, thick black line, Figure 9c) occurs after 15 April 2008. On the basis of equation (9), this cooling is easily accounted for by the additional evaporative loss. Note, however, that our "open ocean" temperature time series θ_{OCN} (thin black line, Figure 9c) shows only a small observable shift, as expected, considering the generally weakly stratified shelf waters in this region. Our well-mixed analytical prediction (thick gray line) is also included in Figure 9c. This should match best with the mean lagoon temperature record, but we include the CTD record (thin gray line) from Figure 2e for additional comparison. The predicted lagoon temperature was constructed using Q_{surf}, θ_{OCN}, and η (all from Figure 9) along with measurements of P (from Figure 2a) and estimates of E from Q_{lat} (as discussed earlier) in equations (8) and (9). Our well-mixed conceptual model captures much of the observed lagoon temperature variability, performing particularly well before 13 April 2008. However, it does fail to provide a perfectly accurate prediction over the entire time series; errors, such as our neglect of Q_{bot}, accumulate with time. Noticeably incorrect are the sudden flood tide transitions observed in the CTD and, to a lesser extent, lagoon-mean temperature records. These features appear similar to the "advective replacement" of lagoon water with ambient ocean water illustrated with our IGW simulations (Figure 7n). We examine these features further in the following section.

[26] To test the accuracy of our surface heat flux estimates and our ability to close the lagoon heat budget with our observations we used the net surface heat flux from Figure 9a and the CTD depth record in equation (9), omitting the $E-P$ term, to predict lagoon mean temperature change. We examined times when the lagoon was isolated from the ocean at low tide (all 2 h durations just before flood) in order to minimize confounding factors such as advection by mean currents. A root-mean square (RMS) deviation between observed and predicted temperature change gave a 22% error when normalized by the observed range of temperature changes. This calculation showed a very slight consistent underprediction of temperature change, suggesting that the CTD depth record may not perfectly reflect the lagoon mean depth. Subtracting 0.05 m from the CTD depth record removed the bias but did not significantly improve the error estimate.

[27] Our conceptual model also under-predicts observed temperature near the midexperiment atmospheric transition, when wind speeds were lowest (Figure 9c). This could result from excessively warm water near the shallow rim, and we do observe analogously cold dips at night consistent with this explanation (see, e.g., the CTD record), though they are not as strong. We suspect that lagoon temperatures at this time were significantly enhanced by a shallow, warm, ambient ocean mixed layer not captured by our θ_{OCN} time series. Such conditions have been linked to significant coral

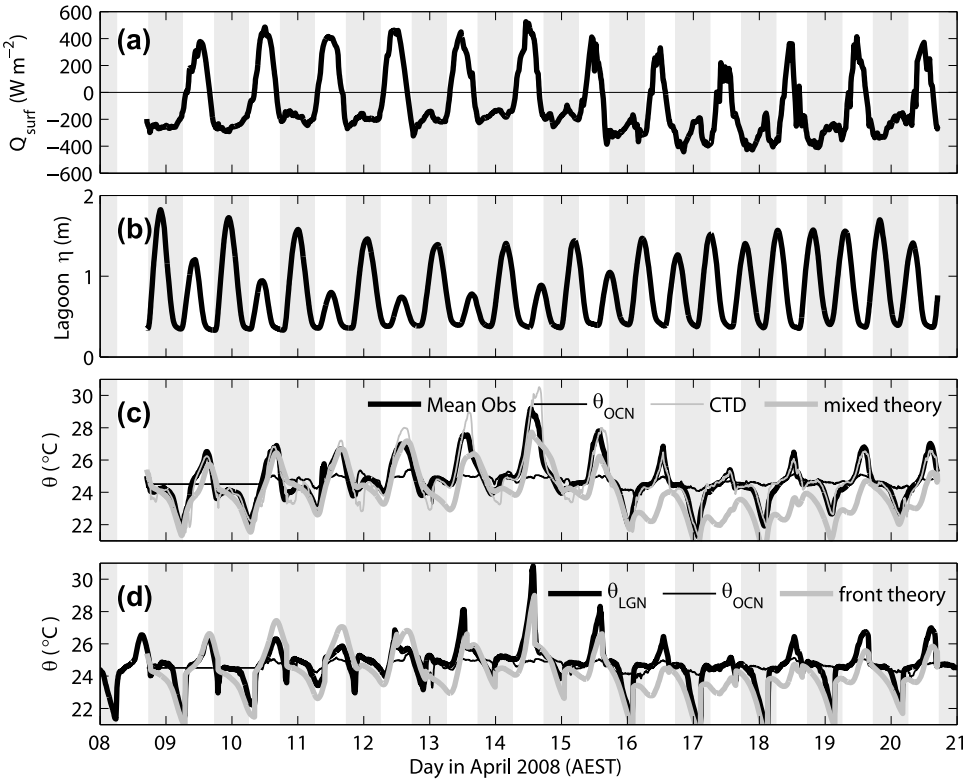

Figure 9. (a) Net surface heat flux Q_{surf} resulting from a sum of all components plotted in Figure 8. (b) Filtered lagoon depth η recorded by the CTD and reproduced from Figure 2d. Figures 9c and 9d include different measures of observed and predicted lagoon temperature. (c) Mean lagoon temperature (thick black line) taken as an average over all lagoon temperature sensors (locations in Figure 10), ambient ocean temperature θ_{OCN} (thin black line) recorded by a temperature sensor at ~2 m depth near the southwest corner of the island (location in Figure 1), temperature recorded by the CTD and reproduced from Figure 2e (thin gray line), and predicted lagoon temperature from our well-mixed conceptual model (thick gray line) using Q_{surf} from Figure 9a, η from Figure 9b, and θ_{OCN} from Figure 9c in equations (8) and (9). We used a constant θ_{OCN} value until midday on 10 April, when the θ_{OCN} temperature sensor was deployed. (d) Observed temperature θ_{LGN} (thick black line) recorded by a single "midlagoon" temperature sensor (location in Figure 1), ambient ocean temperature θ_{OCN} (thin black line) from Figure 9c, and predicted lagoon temperature from our modified frontal model (thick gray line). In this case temperature switches between lagoon volumes when the front is 40% across the lagoon; refer to section 6. Alternating white/gray vertical bands in all panels indicate day/night.

bleaching at other reef sites in the past [*Dennis and Wicklund*, 1993; *Smith*, 2001; *Done et al.*, 2003] and are of primary concern in predicting such events.

6. Flood Tide Thermal Waves and a Modified Frontal Model

6.1. Tidally Forced Thermal Waves

[28] The conceptual model of section 4 was conceived using a control volume to describe variations in mean lagoon temperature by assuming complete and instantaneous mixing of ambient ocean and lagoon water. The model is instructive and captures much of the observed lagoon temperature variability (Figure 9c). However, the well-mixed approach cannot explain the sudden flood tide transitions observed at single locations and in lagoon-average temperature data.

[29] To examine these features further we first present select plan view observations of lagoon temperature throughout a typical tidal cycle in Figure 10. Timing of the individual snapshots is indicated in Figure 10m, and they begin at sunrise on an ebbing tide (Figure 10a). Here relatively warm ocean water has completely filled the LEI lagoon after a nighttime flood and is beginning to flow out of the lagoon with falling sea level. Four hours later (Figure 10b) low tide is reached within the lagoon and resident water has warmed more or less uniformly by about 1°C during the morning hours. Although shallower water near the rim is somewhat warmer (consistent with our above discussion and Figure 6), the ebb tide behavior is largely explained by equation (9). After another 4 h (Figure 10c), the lagoon is excessively warm and lagoon sea level has just started to rise. The beginning of a "thermal wave" is evident at the outer rim, as indicated by the slight reduction in temperature there. The next four snapshots (Figures 10d–10g) are separated by 1 h each and show the progression of this tidally forced thermal wave across the LEI lagoon. Temperature records from individual sensors (Figure 10n) also document the wave's progression across the lagoon and its frontal nature. It takes

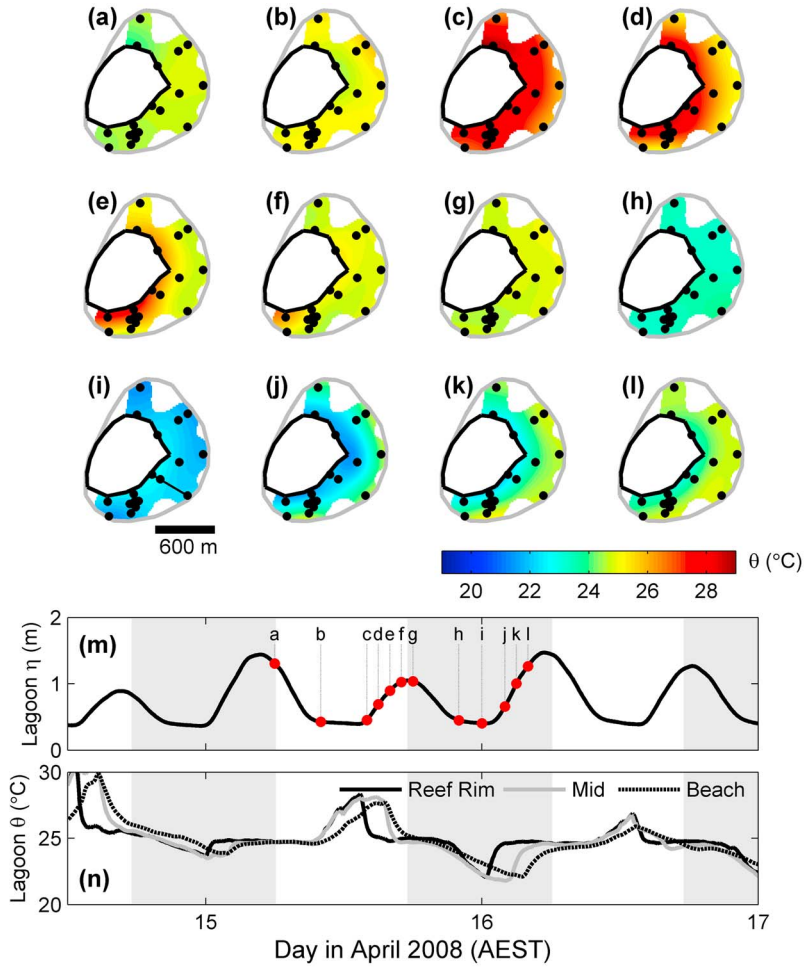

Figure 10. A typical day in the LEI lagoon. (a–l) Plan views of lagoon temperature (°C) observed throughout a tidal cycle. Black dots denote individual temperature sensor locations. (m) The filtered lagoon depth record from the CTD (its lagoon location is the westernmost nearshore dot; see also Figure 1). Lettered labels in Figure 10m indicate the timing of each of the 12 plan view temperature snapshots. (n) Individual temperature time series from three lagoon sensors. Sensor locations are along the line drawn in Figure 10i. A 600 m scale bar is also included beneath Figure 10i for reference.

until high tide (Figure 10g) for the anomalously warm lagoon water to be entirely "replaced" by ocean water. The homogenous state at high tide (Figure 10g) is similar to that just after the previous high tide (Figure 10a). Resident lagoon water then cools considerably (and uniformly, in keeping with our original conceptual model) during the nighttime ebb (Figures 10h and 10i), until another thermal wave of oceanic water inundates it on the following nighttime flood tide (Figures 10j–10l).

[30] The patterns illustrated in Figure 10 share features with both numerical simulations (Figures 6 and 7). Lagoon water appears to be advectively replaced by ambient ocean water as in Figure 7, but the replacement acts quasi-radially, similar to our potential flow case (Figure 6). We do not observe resident lagoon water being swept away by a prevailing current (Figure 7) or the southeast trade winds [*Ludington*, 1979]. Rather, it appears as if the incoming thermal wave slowly displaces resident lagoon water over the course of the flood tide. Of course most our temperature sensors were placed on the lagoon seabed, so it is possible that a cold water intrusion could displace resident lagoon water vertically, allowing it to then be advected away undetected. However, our data shows similar behavior during both the day and nighttime flood tides (Figure 10), suggesting this possibility may not be the case. Lacking additional knowledge of vertical stratification, we proceed by assuming that the entire shallow lagoon water column (0.5–2 m deep) is replaced by the incoming thermal wave of ocean water.

6.2. A Modified Conceptual Approach With Limited Horizontal Mixing

[31] An alternative theoretical approach then is to assume no mixing of the two water masses. In this case, incoming ocean water can completely replace lagoon water, and we ignore the above-mentioned complications of relatively cold ocean water flowing underneath more buoyant lagoon water (or the opposite) and straining of the density field. A schematic representation is given in Figure 11. In this diagnostic scenario, the frontal propagation can be set entirely by geometry. For example, in a two-dimensional rectangular

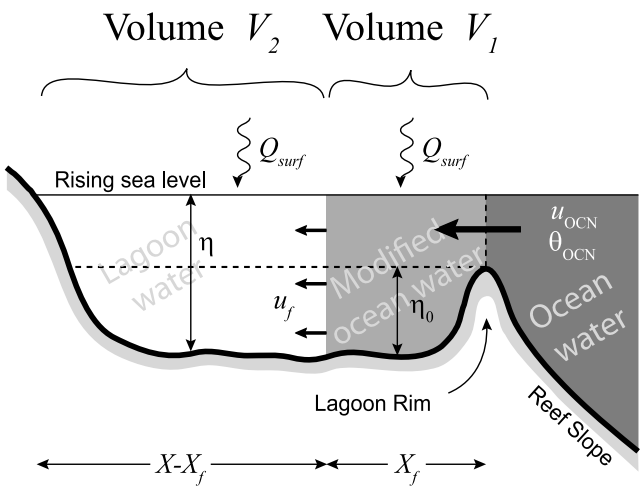

Figure 11. Schematic of the modified flood tide control volume approximation for the LEI lagoon. In this two-dimensional scenario ocean water entering the lagoon does not mix with resident lagoon water. Instead, lagoon water (of volume V_2) is advectively replaced by the propagating thermal front of modified ocean water (volume V_1). In our theoretical treatment, ocean water is strongly modified by surface heat flux once it enters the lagoon; both water volumes are heated by solar energy during the day and they cool at night. The lagoon width is X and the front position relative to the lagoon rim is X_f.

setting, if the cross-lagoon width scale is X and the flood tide lagoon depth is η, then the cross-lagoon front location X_f may be written as

$$X_f = \left(\frac{\eta - \eta_0}{\eta}\right) X, \tag{10}$$

with frontal speed

$$u_f = \frac{\partial X_f}{\partial t} = X \frac{\eta_0}{\eta^2} \frac{\partial \eta}{\partial t}. \tag{11}$$

Equation (10) results from equating the lagoon sea level change to the volume of incoming ocean water. It further implies that equation (11) should be a minimum frontal propagation rate, since it ignores additional contributions such as an internal gravity wave speed and reef rim wave setup. Using these expressions, we can pursue a control volume analysis for each of the two water mass volumes V_1 and V_2 in Figure 11. Radial or annular geometries could also be used to track the frontal propagation, although the control volume analysis would need to be recast in cylindrical coordinates. We pursue a rectangular setting here because of its simplicity. Flood and ebb temperature variability in the nearshore volume V_2 is governed by equation (9) because it does not mix with any new water and only changes depth. Here we retain resident lagoon water within the lagoon. It is straightforward to allow lagoon water to escape V_2, but in that case either the lagoon water's removal rate or the frontal propagation rate would need to be explicitly specified. The outermost volume V_1 is treated as in our original well-mixed model (with incoming ocean water) except now the volume also expands laterally across the lagoon according to equation (10). This amounts to a slight change in the equation governing volume-average temperature evolution, which, after some simplification with equations (10) and (11), may be written as

$$\frac{\partial \theta}{\partial t} + \theta \frac{1}{\eta - \eta_0} \frac{\partial \eta}{\partial t} = \left(\frac{1}{\eta - \eta_0} \frac{\partial \eta}{\partial t} + \frac{E - P}{\eta}\right) \theta_{\mathrm{OCN}} + \frac{1}{\eta} \frac{Q_{\mathrm{surf}}}{\rho_0 c_p}. \tag{12}$$

Equation (12) includes explicit physical dependence on η_0. Its solution may be found using an integrating factor of $\eta - \eta_0$ or equivalently via direct integration realizing that $\partial\eta/\partial t = \partial(\eta - \eta_0)/\partial t$. In practice we use equations (9) and (12) for the shoreward (V_2) and outer (V_1) flood tide volumes, respectively, making an ad hoc switch to only equation (9) for ebb and slack conditions (and specifying a homogeneous lagoon). That is, we begin our ebb tide integration with the final temperature of the outermost volume, despite the fact that our thermal front never reaches land according to equation (10). We stress that this analysis provides no new physical understanding of the encroaching thermal wave. It is, however, the simplest means with which to incorporate sudden temperature transitions within the lagoon, in keeping with our observations (Figure 10). Summarizing the above, we use equation (9) as our homogenous, single-volume, ebb tide equation and split the lagoon into two flood tide volumes obeying equations (9) and (12), respectively.

[32] The nature of this modified frontal analysis means that comparisons are perhaps most relevant at single locations; obeying equation (9) before the thermal front arrives and switching to the temperature of the outer volume and letting it evolve with equation (12) after the front passes. A sharp thermal transition will result if any temperature difference exists between the two volumes. To illustrate this, a comparison with our modified theoretical prediction and temperature recorded at a single "midlagoon" location θ_{LGN} is presented in Figure 9d. In this case the predicted result (thick gray line) switches from the temperature of the inshore volume to that of the outermost volume when $(\eta - \eta_0)/\eta = 0.4$, i.e., when the front is 40% across the lagoon. We use this criterion because it is approximately the cross-lagoon position of the chosen temperature sensor (θ_{LGN}, Figure 1). The modified conceptual model reproduces sudden temperature transitions present in the observations (thick black line, Figure 9d) very well. Additionally, the frontal model does not overshoot temperature minima late in the time series as much as the well-mixed model. In fact, it is perhaps more accurate than the previous model at any given time (compare Figures 9c and 9d). However, it too fails to capture the large daytime peaks in observed lagoon temperature and misses some short-lived, early-evening, low-water minima present in the observations (see, e.g., 9–11 April, Figure 9d). We suspect these discrepancies result from near-rim, very shallow water that heats/cools excessively and is then advected past the temperature sensor during the early flood stages (as discussed earlier and similar to Figure 6 and the situation described by *Hoguane et al.* [1999]). We have not factored such features into either of our conceptual models. Despite these discrepancies, the frontal model clearly captures the sudden lagoon temperature

transitions and reproduces the correct magnitude of day/night heating/cooling.

7. Discussion

7.1. Limitations and Assumptions

[33] Our initial conceptual model involved a horizontally and vertically well-mixed volume. Indeed, this would seem a reasonable assumption for a small and shallow lagoon like that at LEI. In section 5, we illustrated situations in which the horizontally well-mixed assumption may fail. With Figure 10 and section 6, we showed that even the LEI lagoon is not horizontally well-mixed during flood tides because of an inundating thermal wave. Relaxing the well-mixed assumption allowed us to accommodate the thermal waves in a modified frontal model. However, the notion of a relatively small and shallow lagoon remains imbedded in both conceptual models. Ultimately the models are limited to lagoons having a width less than the tidal excursion or less than the effective tidal excursion that results from the presence of an isolating lagoon rim. A better representation of the thermal front would be necessary in wider or deeper lagoons where its propagation may continue beyond slack high water. Our conceptual models did not take into account wind stress, bottom stress, or wave effects such as wave-induced mixing or reef rim and beach wave setup, even though each of these contributes to lagoon mixing. Such factors also likely dictate lagoon circulation and exchange and could play roles in maintaining the observed thermal front. Similarly, our numerical models did not incorporate an island and sloping beach as occurs at LEI. We expect that more realistic simulations including such features may show differing results since the presence of a sloping beach will act much like the reef rim to promote excess heating and cooling. Site specific solar-tidal phasing will greatly alter the lagoon heat response.

[34] Another aspect that we ignored is how alterations in the mean lagoon depth will impact lagoon temperature variability. For example, even our modified frontal model relied on vertically well-mixed volumes. Obviously this assumption will limit predictability as lagoon depth increases and stratification becomes important. *Andrews et al.* [1984] investigated the temporal variability of thermal stratification in a small (200 m × 80 m), moderately deep (20 m) coral reef lagoon in the GBR. Wind and tide induced mixing in that study helped the top 5 m of water to remain relatively unstratified, except during morning heating (e.g., their Figure 3). Thus, under moderate wind and tidal conditions we might expect our vertically well-mixed models to apply best to lagoons no deeper than about 5 m. However, thermal stratification can be important, even in shallow lagoons like LEI. This is particularly true during periods of light winds (e.g., 14 April 2008, Figures 9c and 9d).

7.2. Physical-Biogeochemical Considerations

[35] Corals are unique in that they offer an extremely rough boundary condition capable of effectively trapping water parcels and extracting energy from the flow; the flow over and around them horizontally stirs and vertically mixes the water column. Additional turbulence in the water column facilitates nutrient uptake by enhancing nutrient gradients at cell walls via thinner boundary layers [e.g., *Baird et al.*, 2004]. Coral ecosystems also strongly modify the biogeochemical properties of their environment [*Bates et al.*, 2001]. Many recent studies have examined carbon system measurements at coral reef sites [*Gattuso et al.*, 1997; *Bates et al.*, 2001; *Dai et al.*, 2009], and it is well-established that calcification/dissolution and photosynthesis/respiration rates vary diurnally [e.g., *Nakamura and Nakamori*, 2009]. Water temperature directly modifies gas solubility coefficients. It is clear that hydrodynamic factors need to be carefully considered in such experiments [*Gattuso et al.*, 1997]. Small shallow lagoons like that at LEI may serve well as "natural laboratories" for examining the physical and biogeochemical influences corals introduce to their environment over a rapidly changing, large-amplitude temperature signal. Additionally, such shallow sites may be useful for further studies of coral physiology because the local corals are adapted to high variance in temperature [*Sammarco et al.*, 2006]. Similar locations may even prove valuable as ecological reservoirs under future change.

8. Summary and Conclusions

[36] Temperature time series collected in the small, shallow lagoon of Lady Elliot Island, Great Barrier Reef, Australia, show marked variability over a variety of time scales. In this paper, we have described a simplified, well-mixed conceptual model to relate changes in mean lagoon temperature to net surface heat flux and tidally varying lagoon depth, the two primary forcing components at this location. The model also incorporated a rudimentary ability to account for ambient water masses entering the lagoon from the ocean. With it, we showed the asymmetric flood/ebb response of a shallow lagoon and underscored the importance of the solar-tidal phasing in lagoon heating; midday and midnight low tides can lead to substantial temperature extremes in shallow settings. Simulations from a numerical ocean model with an idealized "atoll" bathymetry and two different forcings illustrated some additional important points. First, horizontal gradients in lagoon temperature were possible over sloping bathymetry [*Monismith et al.*, 2006], and they can be magnified in shallow water. Second, prevailing ocean currents can easily advect resident lagoon water away without substantial localized mixing [*Ludington*, 1979]. This can, in turn, impact lagoon temperature variability by essentially resetting anomalously heated/cooled regions with more moderate temperature water. Comparisons with our conceptual model proved encouraging and were clearly best when the simulations were aligned with the underlying well-mixed assumption. Our model captured the essence of temperature variability in the LEI lagoon but was unable to accurately predict observed lagoon-average temperature evolution in all cases. One shortcoming was that the well-mixed model could not reproduce observed sudden temperature jumps. We showed that these features are dominant and largely result from flood tide thermal waves that slowly progress across the LEI lagoon. An attempt at modifying our conceptual model to account for these tidally driven thermal waves was made by splitting the lagoon into two separate volumes during flood tides. This frontal model successfully captured the sharp temperature changes and led to an overall improvement in predictability but was still unable to accurately simulate all of the observed temperature

variability. Horizontal temperature gradients can be large in shallow systems and we suggest that early-flood discrepancies between the modified frontal model and observations result from anomalously warm/cold water from the extremely shallow rim being advected into the lagoon during the day/night, similar to the situation described by *Hoguane et al.* [1999]. Even extremely shallow settings, where traditional thought might suggest a well-mixed system, can offer much physical complexity.

[37] **Acknowledgments.** We thank the Great Barrier Reef Marine Park Authority for granting permits for this research and for the spatial reef data used in Figure 1. Peter Gash, Wayne Fox, and the staff of both Seair and Lady Elliot Island helped make this project successful. Ben Reineman, Nick Statom, and Greg Nippard provided much assistance in the field. Suggestions from two anonymous reviewers greatly improved this manuscript. This work was supported under Australian Research Council's Discovery Projects funding scheme; project DP0771055 to J.H. Middleton and W.K. Melville, and project DP0557126 to J.H. Middleton, R.W. Griffiths, and A.M. Moore, and from internal SIO funding to W.K. Melville. The views expressed herein are those of the authors and are not necessarily those of the Australian Research Council.

References

Andrews, J. C., W. C. Dunlap, and N. F. Bellamy (1984), Stratification in a small lagoon in the Great Barrier Reef, *Aust. J. Mar. Freshw. Res.*, *35*, 273–284.

Baird, M. E., M. Roughan, R. W. Brander, J. H. Middleton, and G. J. Nippard (2004), Mass-transfer-limited nitrate uptake on a coral reef flat, Warraber Island, Torres Strait, Australia, *Coral Reefs*, *23*, 386–396, doi:10.1007/s00338-004-0404-z.

Baker, A. C., P. W. Glynn, and B. Riegl (2008), Climate change and coral reef bleaching: An ecological assessment of long-term impacts, recovery trends and future outlook, *Est. Coast. Shelf Sci.*, *80*, 435–471, doi:10.1016/j.ecss.2008.09.003.

Bates, N. R., L. Samuels, and L. Merlivat (2001), Biogeochemical and physical factors influencing seawater fCO_2 and air-sea CO_2 exchange on the Bermuda coral reef, *Limnol. Oceanogr.*, *46*(4), 833–846.

Berkelmans, R., G. De'ath, S. Kininmonth, and W. J. Skirving (2004), A comparison of the 1998 and 2002 coral bleaching events on the Great Barrier Reef: Spatial correlation, patterns, and predictions, *Coral Reefs*, *23*, 74–83, doi:10.1007/s00338-003-0353-y.

Brown, B. E., R. P. Dunne, M. S. Goodson, and A. E. Douglas (2002), Experience shapes the susceptibility of a reef coral to bleaching, *Coral Reefs*, *21*(2), 119–126, doi:10.1007/s00338-002-0215-z.

Bryden, H. L., D. Halpern, and R. D. Pillsbury (1980), Importance of eddy heat flux in a heat budget for Oregon coastal waters, *J. Geophys. Res.*, *85*(C11), 6649–6653, doi:10.1029/JC085iC11p06649.

Chapman, D. C. (1985), Numerical treatment of cross-shelf open boundaries in a barotropic coastal ocean model, *J. Phys. Oceanogr.*, *15*, 1060–1075, doi:10.1175/1520-0485(1985)015<1060:NTOCSO>2.0.CO;2.

Chivas, A., J. Chappell, H. Polach, B. Pillans, and P. Flood (1986), Radiocarbon evidence for the timing and rate of island development, beachrock formation and phosphatization at Lady Elliot Island, Queensland, Australia, *Mar. Geol.*, *69*, 273–287.

Cook, C. B., A. Logan, J. Ward, B. Luckhurst, and C. J. Berg Jr. (1990), Elevated temperatures and bleaching on a high latitude coral reef: The 1988 Bermuda event, *Coral Reefs*, *9*, 45–49.

Dai, M., Z. Lu, W. Zhai, B. Chen, Z. Cao, K. Zhou, W.-J. Cai, and C.-T. A. Chen (2009), Diurnal variations of surface seawater pCO_2 in contrasting coastal environments, *Limnol. Oceanogr.*, *54*(3), 735–745.

Dennis, G. D., and R. I. Wicklund (1993), The relationship between environmental factors and coral bleaching at Lee Stocking Island, Bahamas in 1990, in *Proceedings of the Colloquium on Global Aspects of Coral Reefs: Health, Hazards and History*, edited by R. N. Ginsburg, pp. 167–173, Univ. of Miami, Miami, Fla.

Dever, E. P., and S. J. Lentz (1994), Heat and salt balances over the northern California shelf in winter and spring, *J. Geophys. Res.*, *99*(C8), 16,001–16,017, doi:10.1029/94JC01228.

Done, T., E. Turak, M. Wakeford, G. De'ath, S. Kininmonth, S. Wooldridge, R. Berkelmans, and M. Van Oppen (2003), Testing bleaching resistance hypotheses for the 2002 Great Barrier Reef bleaching event, Unpublished report to the Nature Conservancy, *Aust. Inst. Mar. Sci.*, 106 pp.

Dong, C., J. C. McWilliams, and A. F. Shchepetkin (2007), Island wakes in deep water, *J. Phys. Oceanogr.*, *37*, 962–981, doi:10.1175/JPO3047.1.

Estrade, P., and J. H. Middleton (2010), A numerical study of island wake generated by an elliptical tidal flow, *Cont. Shelf Res.*, *30*, 1120–1135, doi:10.1016/j.csr.2010.03.002.

Fabricius, K. E. (2006), Effects of irradiance, flow, and colony pigmentation on the temperature microenvironment around corals: Implications for coral bleaching? *Limnol. Oceanogr.*, *51*(1), 30–37.

Fairall, C. W., E. F. Bradley, D. P. Rogers, J. B. Edson, and G. S. Young (1996), Bulk parameterization of air-sea fluxes for Tropical Ocean-Global Atmosphere Coupled-Ocean Atmosphere Response Experiment, *J. Geophys. Res.*, *101*(C2), 3747–3764, doi:10.1029/95JC03205.

Feely, R. A., C. L. Sabine, K. Lee, W. Berelson, J. Kleypas, V. J. Fabry, and F. J. Millero (2004), Impact of anthropogenic CO_2 on the $CaCO_3$ system in the oceans, *Science*, *305*, 362–366, doi:10.1126/science.1097329.

Flather, R. A. (1976), A tidal model of the northwest European continental shelf, *Mem. Soc. Roy. Sci. Liege, Ser.*, *6*(10), 141–164.

Flood, P. G., S. Harjanto, and G. R. Orme (1979), Carbon-14 dates, Lady Elliot Reef, Great Barrier Reef, *Qld. Govt. Mining J.*, *80*, 444–447.

Gattuso, J.-P., C. E. Payri, M. Pichon, B. Delesalle, and M. Frankignoulle (1997), Primary production, calcification, and air-sea CO_2 fluxes of a macroalgal-dominated coral reef community (Moorea, French Polynesia), *J. Phycol.*, *33*, 729–738.

Griffin, D. A., and J. H. Middleton (1986), Coastal-trapped waves behind a large continental shelf island, southern Great Barrier Reef, *J. Phys. Oceanogr.*, *16*, 1651–1664, doi:10.1175/1520-0485(1986)016<1651:CTWBAL>2.0.CO;2.

Griffin, D. A., J. H. Middleton, and L. Bode (1987), The tidal and longer-period circulation of Capricornia, southern Great Barrier Reef, *Aust. J. Mar. Freshw. Res.*, *38*, 461–474.

Haidvogel, D. B., H. G. Arango, K. Hedstrom, A. Beckmann, P. Malanotte-Rizzoli, and A. F. Shchepetkin (2000), Model evaluation experiments in the North Atlantic Basin: Simulations in nonlinear terrain-following coordinates, *Dyn. Atmos. Oceans*, *32*, 239–281.

Heath, R. A. (1977), Heat balance in a small coastal inlet Pauatahanui Inlet, North Island, New Zealand, *Est. Coast. Mar. Sci.*, *5*, 783–792.

Heatwole, H. (1984), The cays of the Capricornia section, Great Barrier Reef Marine Park, and a history of research on their terrestrial biota, in *The Capricornia Section of the Great Barrier Reef: Past, Present, and Future*, edited by W. T. Ward and P. Saenger, pp. 25–44, R. Soc. Queen. Aust. Coral Reef Soc. Symp., Brisbane.

Hoegh-Guldberg, O. (1999), Climate change, coral bleaching and the future of the world's coral reefs, *Mar. Freshw. Res.*, *50*, 839–866, doi:10.1071/MF99078.

Hoguane, A. M., A. E. Hill, J. H. Simpson, and D. G. Bowers (1999), Diurnal and tidal variation of temperature and salinity in the Ponta Rasa mangrove swamp, Mozambique, *Est. Coast. Shelf Sci.*, *49*, 251–264.

Jimenez, I. M., M. Kuhl, A. W. D. Larkum, and P. J. Ralph (2008), Heat budget and thermal microenvironment of shallow-water corals: Do massive corals get warmer than branching corals? *Limnol. Oceanogr.*, *53*(4), 1548–1561.

Kleypas, J. A., and D. M. Burrage (1994), Satellite observations of circulation in the southern Great Barrier Reef, Australia, *Int. J. Remote Sens.*, *15*(10), 2051–2063.

Kleypas, J. A., R. W. Buddemeier, D. Archer, J.-P. Gattuso, C. Langdon, and B. N. Opdyke (1999), Geochemical consequences of increased atmospheric carbon dioxide on coral reefs, *Science*, *284*, 118–120, doi:10.1126/science.284.5411.118.

Kleypas, J. A., R. A. Feely, V. J. Fabry, C. Langdon, C. L. Sabine, and L. L. Robbins (2006), *Impacts of ocean acidification on coral reefs and other marine calcifiers: A guide for future research*, 88 pp., U.S. Geol. Survey, St. Petersburg, Fla.

Kjerfve, B. (1978), Diurnal energy balance of a Caribbean barrier reef environment, *Bull. Mar. Sci.*, *28*(1), 137–145.

Kundu, P. K., and I. M. Cohen (2008), *Fluid Mechanics*, 4th ed., 872 pp., Academic, San Diego.

Leinweber, A., N. Gruber, H. Frenzel, G. E. Friederich, and F. P. Chavez (2009), Diurnal carbon cycling in the surface ocean and lower atmosphere of Santa Monica Bay, California, *Geophys. Res. Lett.*, *36*, L08601, doi:10.1029/2008GL037018.

Lentz, S. J. (1987), A heat budget for the northern California shelf during CODE 2, *J. Geophys. Res.*, *92*(C13), 14,491–14,509, doi:10.1029/JC092iC13p14491.

Ludington, C. A. (1979), Tidal modifications and associated circulation in a platform reef lagoon, *Aust. J. Mar. Freshw. Res.*, *30*, 425–430.

Marchesiello, P., J. C. McWilliams, and A. Shchepetkin (2001), Open boundary conditions for long-term integration of regional oceanic models, *Ocean Modell.*, *3*, 1–20.

Marshall, P. A., and A. H. Baird (2000), Bleaching of corals on the Great Barrier Reef: Differential susceptibilities among taxa, *Coral Reefs*, *19*, 155–163.

Maynard, J. A., et al. (2008), ReefTemp: An interactive monitoring system for coral bleaching using high-resolution SST and improved stress predictors, *Geophys. Res. Lett.*, *35*, L05603, doi:10.1029/2007GL032175.

Merrifield, M. A., and J. H. Middleton (1994), The influence of strongly varying topography on coastal-trapped waves at the southern Great Barrier Reef, *J. Geophys. Res.*, *99*(C5), 10,193–10,205, doi:10.1029/94JC00361.

Middleton, J. H., P. Coutis, D. A. Griffin, A. Macks, A. McTaggart, M. A. Merrifield, and G. J. Nippard (1994), Circulation and water mass characteristics of the southern Great Barrier Reef, *Aust. J. Mar. Freshw. Res.*, *45*, 1–18.

Monismith, S. G., A. Genin, M. A. Reidenbach, G. Yahel, and J. R. Koseff (2006), Thermally driven exchanges between a coral reef and the adjoining ocean, *J. Phys. Oceanogr.*, *36*, 1332–1347, doi:10.1175/JPO2916.1.

Monismith, S. G., J. L. Hench, D. A. Fong, N. J. Nidzieko, W. E. Fleenor, L. P. Doyle, and S. G. Schladow (2009), Thermal variability in a tidal river, *Estuaries Coasts*, *32*, 100–110, doi:10.1007/s12237-008-9109-9.

Munk, W. H., and M. C. Sargent (1948), Adjustment of Bikini Atoll to ocean waves, *Eos. Trans. AGU*, *29*(6), 855–860.

Nakamura, T., and T. Nakamori (2009), Estimation of photosynthesis and calcification rates at a fringing reef by accounting for diurnal variations and the zonation of coral reef communities on reef flat and slope: A case study for the Shiraho reef, Ishigaki Island, southwest Japan, *Coral Reefs*, *28*, 229–250, doi:10.1007/s00338-008-0454-8.

Nakamura, T., and R. van Woesik (2001), Water-flow rates and passive diffusion partially explain differential survival of corals during the 1998 bleaching event, *Mar. Ecol. Prog. Ser.*, *212*, 301–304.

Pawlowicz, R., B. Beardsley, S. Lentz, E. Dever, and A. Anis (2001), Software simplifies air-sea data estimates, *Eos Trans. AGU*, *82*(1), 2.

Pawlowicz, R., B. Beardsley, and S. Lentz (2002), Classical tidal harmonic analysis including error estimates in MATLAB using T_TIDE, *Comput. Geosci.*, *28*(8), 929–937.

Reineman, B. D., L. Lenain, D. Castel, and W. K. Melville (2009), A portable airborne scanning Lidar system for ocean and coastal applications, *J. Atmos. Ocean. Tech.*, *26*, 2626–2641, doi:10.1175/2009JTECHO703.1.

Sammarco, P. W., A. Winter, and J. C. Stewart (2006), Coefficient of variation of sea surface temperature (SST) as an indicator of coral bleaching, *Mar. Biol.*, *149*, 1337–1344, doi:10.1007/s00227-006-0318-0.

Shchepetkin, A. F., and J. C. McWilliams (2005), The regional oceanic modeling system (ROMS): A split-explicit, free surface, topography-following-coordinate oceanic model, *Ocean Modell.*, *9*, 347–404, doi:10.1016/j.ocemod.2004.08.002.

Smith, N. P. (2001), Weather and hydrographic conditions associated with coral bleaching: Lee Stocking Island, Bahamas, *Coral Reefs*, *20*, 415–422, doi:10.1007/s00338-001-0189-2.

Smith, N. P., and G. H. Kierspe (1981), Local energy exchanges in a shallow coastal lagoon: Winter conditions, *Est. Coast. Shelf Sci.*, *13*, 159–167.

Smithers, B. V., D. R. Peck, A. K. Krockenberger, and B. C. Congdon (2003), Elevated sea-surface temperature, reduced provisioning and reproductive failure of wedge-tailed shearwaters (*Puffinus pacificus*) in the southern Great Barrier Reef, Australia, *Mar. Freshw. Res.*, *54*(8), 973–977, doi:10.1071/MF02137.

Stewart, R. H. (2008), *Introduction to physical oceanography*, 345 pp., Texas A&M Univ., College Station, Tex. (Available at http://ocean-world.tamu.edu/resources/ocng_textbook/PDF_files/book_pdf_files.html).

Uncles, R. J., and J. A. Stephens (2001), The annual cycle of temperature in a temperate estuary and associated heat fluxes to the coastal zone, *J. Sea. Res.*, *46*, 143–159.

Vugts, H. F., and J. T. F. Zimmerman (1975), Interaction between the daily heat balance and the tidal cycle, *Nature*, *255*(5504), 113–117, doi:10.1038/255113a0.

Warner, J., R. Signell, and H. Arango (2006), Incorporating nearshore processes into ROMS, *Eos Trans. AGU*, *87*(36), Ocean Sci. Meet. Suppl., Abstract OS35D-01.

Weeks, S. J., K. R. N. Anthony, A. Bakun, G. C. Feldman, and O. Hoegh-Guldberg (2008), Improved predictions of coral bleaching using seasonal baselines and higher spatial resolution, *Limnol. Oceanogr.*, *53*(4), 1369–1375.

Weller, E., M. Nunez, G. Meyers, and I. Masiri (2008), A climatology of ocean-atmosphere heat flux estimates over the Great Barrier Reef and Coral Sea: Implications for recent mass coral bleaching events, *J. Clim.*, *21*, 3853–3871, doi:10.1175/2007JCLI2085.1.

West, J. M., and R. V. Salm (2003), Implications for coral reef conservation and management, *Conserv. Biol.*, *17*(4), 956–967.

Wilkin, J. L. (2006), The summertime heat budget and circulation of southeast New England shelf waters, *J. Phys. Oceanogr.*, *36*, 1997–2011, doi:10.1175/JPO2968.1.

Wilkin, J. L., and D. C. Chapman (1990), Scattering of coastal-trapped waves by irregularities in coastline and topography, *J. Phys. Oceanogr.*, *20*, 396–421, doi:10.1175/1520-0485(1990)020<0396:SOCTWB>2.0.CO;2.

Wooldridge, S., and T. Done (2004), Learning to predict large-scale coral bleaching from past events: A Bayesian approach using remotely sensed data, in situ data, and environmental proxies, *Coral Reefs*, *23*, 96–108, doi:10.1007/s00338-003-0361-y.

Yates, K. K., C. Dufore, N. Smiley, C. Jackson, and R. B. Halley (2007), Diurnal variation of oxygen and carbonate system parameters in Tampa Bay and Florida Bay, *Mar. Chem.*, *104*, 110–124, doi:10.1016/j.marchem.2006.12.008.

P. Estrade and J. H. Middleton, Department of Aviation, University of New South Wales, Sydney, NSW 2052, Australia.

L. Lenain and W. K. Melville, Scripps Institution of Oceanography, University of California San Diego, La Jolla, CA 92093-0213, USA.

R. M. McCabe, School of Oceanography, University of Washington, Box 355351, Seattle, WA 98195, USA. (rmccabe@ocean.washington.edu)

M. Roughan, University of New South Wales, School of Mathematics and Statistics, Sydney, NSW 2052, Australia.